Sensorless Position Estimation of Electro-Hydraulic Proportional Valve Using Dual Solenoids

Jiasheng Wang, Qi Su*, Junhui Zhang, Xukun Zhang, Jinheng Liu, and Zhi Qiu

State Key Laboratory of Fluid Power and Mechatronic Systems, Zhejiang University, Hangzhou, China
E-mail: zjuwjs@zju.edu.cn, suqi@zju.edu.cn, benzjh@zju.edu.cn, zhangxk987@163.com, ljh1640914541@163.com, qiuzhi@zju.edu.cn

Abstract

Solenoid-actuated valves used in construction machinery are typically not equipped with position sensors to reduce costs. This hinders the acquisition of spool position information during operation and adversely affects degradation prediction and fault diagnosis. This study presents a soft measurement method for spool position estimation in solenoid-actuated valves without position sensors. The technique utilizes the position information fusion of the two solenoids in the valve. First, a spool displacement model is derived based on the inductance variations of the working solenoid, and the solenoid simulation model is established using data from the solenoid tests and the measurement of the solenoid structure. Meanwhile, a high-frequency excitation signal is applied to the idle solenoid, and feedback from the circuit is utilized to measure changes in inductance, allowing for the derivation of the spool position. Subsequently, an improved adaptive Kalman filter algorithm is developed to fuse these two position estimates, establishing an adaptive soft measurement model for dynamic spool position estimation. Finally, simulation validation is conducted on a Simulink model based on the proposed method. The results indicate that the proposed position estimation method can achieve high-precision spool position information over the full spool stroke.

Keywords: Proportional valve, Soft measurement, Position estimation, Solenoid inductance, Kalman filter

1 Introduction

Solenoid-actuated valves are widely used in construction equipment, agricultural machinery, and mining machinery [1]. Therefore, these valves often operate under conditions of significant vibration and harsh working environments. Moreover, due to cost constraints, it is challenging to equip precise displacement sensors, e.g., linear variable displacement transducer (LVDT), in solenoid-actuated valves, which hinders the acquisition of valve spool position information [2]. Currently, these machines predominantly depend on the operator's experiential knowledge for their operation. For example, adjusting the position of components, such as the terminal section of excavating machinery, relies heavily on the operator's visual perception. This reliance substantially hinders the advancement of automation in construction and production processes, as well as the development of effective fault diagnosis methods. Therefore, the research on position soft measurement for solenoid-actuated valves is of great significance.

In recent years, soft measurement technology, an indirect measurement technique where a mathematical model or algorithm is used to estimate a process variable based on other available sensor data rather than measuring it directly, has been gradually applied to hydraulic actuators [3-5]. By exploiting the inherent correlations between internal parameters of controlled systems, the estimation of critical states by mathematical models or data-driven approaches can effectively reduce the dependence on traditional sensors. In electrohydraulic valve applications, proportional solenoids have been widely adopted due to their cost-effectiveness, high output force, and favorable linearity [6]. There is a clear functional relationship between the air gap length of the solenoid and its inductance value, which provides both the theoretical basis and the technical path for position sensing. Existing electromagnetic position soft sensing methods can be categorized into three classes. The first category targets low-speed applications, including inductance-based position estimation via pulse injection, current waveform monitoring for position inference, and methods utilizing switching signals from power electronics hardware [7]. Nagai et al [8] developed a low-cost position and force sensing strategy for compact solenoid actuators by superimposing an alternating current (AC) component on a direct current (DC) power supply. This enables simultaneous real-time estimation of position and force. Their subsequent work [9] implemented inductance-displacement soft sensing combined with disturbance observer

control for dual solenoids. Considering the ambiguities caused by hysteresis and saturation effects, Kramer et al [10] proposed a self-sensing design of the proportional solenoids, which balances the force generation ability and the sensor properties. The second category focuses on medium to high speed scenarios and typically incorporates observer-based position estimation and neural network approaches that establish mappings between position, magnetic flux, and current [11]. Zhao et al [12] achieved sensorless linear control of spool position in electromagnetic switching valves by integrating sliding mode controllers with nonlinear sliding mode observers. The third category employs auxiliary components for position estimation, predominantly in motor applications, such as additional stator coils for current variation detection, bootstrap circuits for initial mover positioning, eddy current sensors that correlate signals with position, and dedicated sensing units with auxiliary stator/rotor laminations [13]. Jing et al [14] realized gap self-inductance sensing in maglev systems using an auxiliary coil with high-frequency excitation, demonstrating enhanced sensitivity in suspension gap measurement. Verma et al [15] proposed a self-sensing electromagnetic actuator for vibration suppression in flexible structures, where structural displacement was evaluated by back electromotive force measurements in the coil.

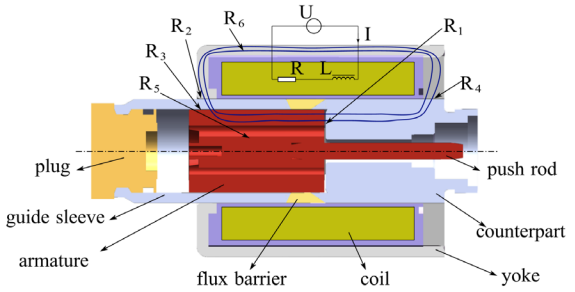

Figure 1: Structure of the electrohydraulic proportional solenoid

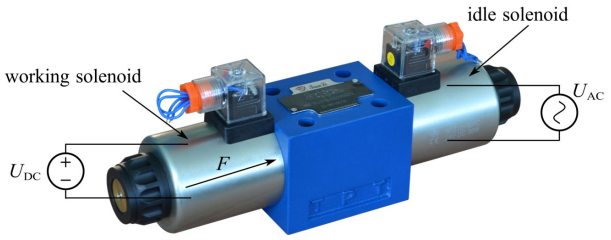

Figure 2: Working principle of dual solenoids in a valve

Based on the low speed and auxiliary component methodology, this study proposes a soft measurement method for spool position in electrohydraulic proportional valves with the collaborative operation of dual solenoids. Fig. 1 illustrates the structure of the proportional solenoid adopted in this paper. During directional valve operation, one working solenoid is typically energized to generate force while the other remains idle, as shown in fig. 2. Firstly, during high-current force generation, the working solenoid achieves self-sensing by exploiting the relationship between inherent inductance and air gap, enabling real-time position monitoring during actuation. Meanwhile, the idle solenoid will be used to serve as an auxiliary sensing component for position monitoring. Sinusoidal excitation signals are applied to the idle solenoid, and the air gap-inductance relationship is pre-calibrated. Displacement information is inversely derived from inductance values calculated under sinusoidal excitation. Finally, an adaptive Kalman filtering algorithm merges the two displacement estimates to obtain the final measurement.

The major innovations of this study are summarized as follows:

(1) Dual-solenoid position soft measurement method. A novel soft sensing strategy using coordinated dual-solenoid operation is proposed: The working solenoid simultaneously performs thrust generation and self-sensing functions, thus achieving integration of displacement measurement and actuation. The idle solenoid enables real-time spool displacement inversion through sinusoidal excitation signal injection and pre-calibrated inductance between air gap relationships. In particular, the initial position of the working solenoid is obtained directly through step excitation without the need for additional inductance and position calibration.

(2) An adaptive Kalman filter is designed to perform data fusion, which enhances measurement accuracy and noise immunity. The precision of the dual-solenoid method shows better results than the single-solenoid soft measurement methods. The position soft measurement method works with existing solenoid structures without additional components, ensuring full compatibility with standard electromagnetic valve operation.

The methodological framework of this study is organized as follows: Section 2 presents the proposed approach in detail. Section 3 describes the experimental data acquisition setup and the established simulation model for the validation simulations to be performed. Section 4 analyzes the results of the simulations and their practical implications. Section 5 summarizes the results of the study, discusses limitations, and suggests directions for future research. Finally, all symbols used in this paper are listed and defined in the Nomenclature section.

2 Principle of dual-solenoid position soft measurement

2.1 Position self-sensing method for working solenoid

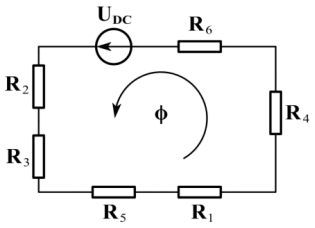

Figure 3: Magnetic circuit of the solenoid

The magnetic circuit characteristics of the working solenoid are shown in fig. 3, and the analysis of the reluctance positions is annotated in fig. 1. The relationship between magnetic reluctance and air gap dimensions is as follows:

$$R_1 = \frac{x_1}{\mu_0 A_s} \tag{1}$$

$$R_2 = \int_{r_{22}}^{r_{21}} \frac{dr}{2\pi r \mu_0 l_2} = \frac{\ln(r_{21}/r_{22})}{2\pi\mu_0 l_2} \tag{2}$$

$$R_3 = \int_{r_{32}}^{r_{31}} \frac{dr}{2\pi r \mu_0 l_3} = \frac{\ln(r_{31}/r_{32})}{2\pi\mu_0 l_3} \tag{3}$$

$$R_4 = \int_{r_{42}}^{r_{41}} \frac{dr}{2\pi r \mu_0 l_4} = \frac{\ln(r_{41}/r_{42})}{2\pi\mu_0 l_4} \tag{4}$$

Since the solenoid is a wet-type solenoid, the theoretical magnetic permeability u_0 is that of hydraulic oil. However, commonly used hydraulic oils are non-magnetic fluids, and their magnetic permeability is similar to that of air. In this study, $u_0 = 4\pi \times 10^{-7}$ H/m. Due to the significantly higher magnetic permeability of the metal components of the solenoid compared to air, the effects of the metal reluctances R_5 and R_6 can be neglected. The structure parameters of the solenoid satisfy $r_{21} = r_{41}$, $r_{22} = r_{42}$, and $l_2 = l_4$. Therefore, $R_2 = R_4$.

According to Kirchhoff's second law:

$$NI_w = \phi_1 (R_1 + R_2 + R_3 + R_4 + R_5 + R_6) \tag{5}$$

and the definition of self-inductance in electromagnetism:

$$\psi = N\phi_1 = L_w I_w \tag{6}$$

It follows:

$$\begin{aligned} L_w &= \frac{N\phi_1}{I_w} \\ &= \frac{N}{I_w} \times \frac{NI_w}{R_1 + R_2 + R_3 + R_4 + R_5 + R_6} \\ &\approx \frac{N^2}{R_1 + 2R_2 + R_3} \end{aligned} \tag{7}$$

During the operation of the solenoid, there are

$$U_{DC} = U_L + U_R \tag{8}$$

$$U_R = I_w R \tag{9}$$

$$U_L = U_{DC} - I_w R \tag{10}$$

$$\psi_0 = \int_0^{t_0} U_L(t)\,dt \tag{11}$$

Since the solenoid operates in the non-saturation region, combining eq. (6) and eq. (11), it follows:

$$L_0 = \frac{\psi_0}{i_0} \tag{12}$$

Combining eq. (7), it follows:

$$L_0 = \frac{N^2}{\frac{\delta_0}{\mu_0 A_s} + \frac{\ln(r_{21}/r_{22})}{\pi\mu_0 l_2} + \frac{\ln(r_{31}/r_{32})}{2\pi\mu_0 l_3}} = \frac{\psi_0}{i_0} \tag{13}$$

The initial position δ_0 can be calculated based on the given parameters.

$$\delta_0 = A_s \left(\frac{\mu_0 N^2 i_0}{\psi_0} - \frac{\ln(r_{21}/r_{22})}{\pi l_2} - \frac{\ln(r_{31}/r_{32})}{2\pi l_3} \right) \tag{14}$$

The magnetic flux $\Delta\psi$ of the solenoid is:

$$\Delta\psi = \int_{t_0}^{t_0+\Delta t} U_L(t)\,dt \tag{15}$$

From eq. (6), it follows:

$$d\psi = dLi = L\,di + i\,dL \tag{16}$$

Therefore, based on the iterative method for calculating the real-time inductance:

$$\begin{cases} L_1 = \dfrac{\Delta\psi - L_0 \Delta i}{i_0} + L_0 \\ \quad\quad ... \\ L_k = \dfrac{\Delta\psi - L_{k-1}\Delta i}{i_{k-1}} + L_{k-1} \end{cases} \tag{17}$$

and

$$L_k = \frac{N^2}{\frac{\delta_0 + \Delta x}{\mu_0 A_s} + \frac{\ln(r_{21}/r_{22})}{\pi\mu_0 l_2} + \frac{\ln(r_{31}/r_{32})}{2\pi\mu_0 l_3}} \tag{18}$$

By solving eq. (18), the iron core position x_1 is:

$$\begin{aligned} x_1 &= \delta_0 + \Delta x \\ &= A_s \left(\frac{\mu_0 N^2}{\frac{\Delta\psi - L_{k-1}\Delta i}{i_{k-1}} + L_{k-1}} - \frac{\ln(r_{21}/r_{22})}{\pi l_2} - \frac{\ln(r_{31}/r_{32})}{2\pi l_3} \right) \end{aligned} \tag{19}$$

2.2 Position estimation method for idle solenoid

When a sinusoidal voltage excitation is applied to the idle solenoid, the following relationship applies:

$$U_{AC} = \bar{U}_m \sin(\omega t) + U_k \tag{20}$$

The solenoid current will also have sinusoidal fluctuations:

$$I_{AC} = \bar{I}_m \sin(\omega t - \theta) + I_k \tag{21}$$

The solenoid voltage equation is:

$$\begin{aligned} U_{AC} &= I_{AC} R + \frac{d\phi_2}{dt} \\ &= I_{AC} R + I_{AC} \frac{dL_s}{dt} + L_s \frac{dI_{AC}}{dt} \end{aligned} \tag{22}$$

When the current is small, the inductance has a one-to-one correspondence with the position [10], it follows:

$$U_{AC} = I_{AC} R + L_s \frac{dI_{AC}}{dt} \tag{23}$$

By combining eq. (20), eq. (21), and eq. (23), it follows:

$$\begin{aligned} &\bar{U}_m \sin(\omega t) + U_k \\ &= \bar{I}_m \sqrt{R^2 + (\omega L_s)^2} \sin(\omega t - \theta + \theta') + I_k R \end{aligned} \tag{24}$$

where

$$\theta' \in \left(-\frac{\pi}{2}, \frac{\pi}{2}\right),\ \tan\theta' = \frac{\omega L_s}{R},\ U_k = I_k R$$

By equating the corresponding terms, it can be concluded that

$$\theta = \theta', \ \bar{U}_{\mathrm{m}} = \bar{I}_{\mathrm{m}} \sqrt{R^2 + (\omega L_{\mathrm{s}})^2}$$

Therefore, the L_{s} is as follows:

$$L_{\mathrm{s}} = \frac{1}{\omega} \sqrt{\left(\frac{\bar{U}_{\mathrm{m}}}{\bar{I}_{\mathrm{m}}}\right)^2 - R^2} \tag{25}$$

The relationship between core position and inductance is calibrated beforehand for the idle solenoid used in this paper, and a fitted relationship is established:

$$x_2 = aL_{\mathrm{s}}^4 + bL_{\mathrm{s}}^3 + cL_{\mathrm{s}}^2 + dL_{\mathrm{s}} + e \tag{26}$$

Based on this equation, the real-time position of the solenoid iron core can be obtained.

2.3 Adaptive Kalman filter algorithm

(1) The first step is to build the state model. Defining the state vector:

$$X_{\mathrm{k}} = \begin{bmatrix} x_{\mathrm{k}} \\ v_{\mathrm{k}} \end{bmatrix} \tag{27}$$

In a discrete-time system with sampling period T, the state transition model is:

$$x_{\mathrm{k}} = Ax_{\mathrm{k}-1} + w_{\mathrm{k}-1}, \ w_{\mathrm{k}-1} \sim N(0, Q_{\mathrm{k}}) \tag{28}$$

where the state transition matrix A is:

$$A = \begin{bmatrix} 1 & T \\ 0 & 1 \end{bmatrix} \tag{29}$$

(2) The second step is to build the observation model. The system has two measurement signals: $z_{1,\mathrm{k}}$ (working solenoid position x_1 calculated from the solenoid model) and $z_{2,\mathrm{k}}$ (idle solenoid position x_2 derived from a sensor-like method). The observation matrix C is defined as:

$$C = \begin{bmatrix} 1 & 0 \\ 1 & 0 \end{bmatrix} \tag{30}$$

The observation equation is:

$$z_{\mathrm{k}} = Cx_{\mathrm{k}} + r_{\mathrm{k}}, \ r_{\mathrm{k}} \sim N(0, R_{\mathrm{k}}) \tag{31}$$

The initial observation noise covariance is:

$$R_{\mathrm{base}} = \begin{bmatrix} r_{\mathrm{base}\,1} & 0 \\ 0 & r_{\mathrm{base}\,2} \end{bmatrix} \tag{32}$$

(3) Adaptive adjustment of noise covariance design. First, the observation noise covariance R_{k} is dynamically modified. Since the inductance L_{w} is calculated iteratively in the self-sensing model of the working solenoid, the position estimation $z_{1,\mathrm{k}}$ may become unreliable during abrupt position changes (e.g., step). To mitigate the impact of $z_{1,\mathrm{k}}$ inaccuracies, increase the confidence in $z_{2,\mathrm{k}}$. Adjust R_{k} based on the discrepancy between $z_{1,\mathrm{k}}$ and $z_{2,\mathrm{k}}$:

$$R_{\mathrm{k}} = \begin{cases} mR_{\mathrm{base}}, & \text{if } |z_{2,\mathrm{k}} - z_{1,\mathrm{k}}| > x_{\mathrm{Ru}}, \\ nR_{\mathrm{base}}, & \text{if } |z_{2,\mathrm{k}} - z_{1,\mathrm{k}}| < x_{\mathrm{Rl}}, \\ R_{\mathrm{base}}, & \text{otherwise.} \end{cases} \tag{33}$$

A dynamic adjustment for the process noise Q_{k} is then performed. Since the idle solenoid only plays an auxiliary role in position measurement during the process, it cannot be subjected to an excitation voltage that is too high to avoid generating a magnetic force that would affect the control of the solenoid valve. Therefore, the response current of the idle solenoid is generally small, within 30 mA. The current acquisition circuit has limited accuracy and is susceptible to external interference. It is necessary to process the noise of the idle solenoid position estimation. The noise is dynamically updated according to the deviation $\mathrm{d}x_2$, of x_2 from the current estimate:

$$Q_k = \begin{cases} \begin{bmatrix} q_{\mathrm{k}1} & 0 \\ 0 & q_{\mathrm{k}2} \end{bmatrix}, & \text{if } \mathrm{d}x_2 > x_{\mathrm{Qu}}, \\ \begin{bmatrix} q_{\mathrm{k}3} & 0 \\ 0 & q_{\mathrm{k}4} \end{bmatrix}, & \text{if } \mathrm{d}x_2 < x_{\mathrm{Ql}}, \\ \begin{bmatrix} q_{\mathrm{k}5} & 0 \\ 0 & q_{\mathrm{k}6} \end{bmatrix}, & \text{otherwise.} \end{cases} \tag{34}$$

When x_2 varies drastically, increasing Q_{k} allows the filter to track abrupt changes more quickly. When x_2 is smooth, decreasing Q_{k} improves smoothing.

(4) A fusion factor α is designed to fuse the data of x_1 and x_2 weightedly. Define the step error as

$$s_{\mathrm{err}} = |z_{1,\mathrm{k}} - \hat{x}_{\mathrm{k}-1}| \tag{35}$$

and the noise level as

$$n_{\mathrm{L}} = |z_{2,\mathrm{k}} - \hat{x}_{\mathrm{k}-1}| \tag{36}$$

Calculate the fusion factor there:

$$\alpha = 1 - \frac{n_{\mathrm{L}}}{n_{\mathrm{L}} + s_{\mathrm{err}} + \varepsilon} \tag{37}$$

If $z_{2,\mathrm{k}}$ has higher noise levels and $z_{1,\mathrm{k}}$ is more stable, α tends to 0, relying more on data from x_1. If $z_{2,\mathrm{k}}$ differs less from the current estimate (low noise) and $z_{1,\mathrm{k}}$ differs more from the current estimate, α tends to 1, relying mainly on measurements from x_2. A weighted fusion of the position components in the state:

$$\hat{x}_{\mathrm{k}} = \alpha \hat{x}_{\mathrm{k}} + (1 - \alpha) z_{1,\mathrm{k}} \tag{38}$$

(5) Synthesize the above design scheme to update the Kalman filter. Its prediction steps are:

$$\hat{x}_{\mathrm{k}|\mathrm{k}-1} = A\hat{x}_{\mathrm{k}-1|\mathrm{k}-1} \tag{39}$$

$$P_{\mathrm{k}|\mathrm{k}-1} = AP_{\mathrm{k}-1|\mathrm{k}-1}A^{\mathrm{T}} + Q_{\mathrm{k}} \tag{40}$$

The Kalman gain calculation in data updating is as follows:

$$K_{\mathrm{k}} = P_{\mathrm{k}|\mathrm{k}-1}C^{\mathrm{T}} \left(CP_{\mathrm{k}|\mathrm{k}-1}C^{\mathrm{T}} + R_{\mathrm{k}}\right)^{-1} \tag{41}$$

The status update will be as follows:

$$\hat{x}_{\mathrm{k}|\mathrm{k}} = \hat{x}_{\mathrm{k}|\mathrm{k}-1} + K_{\mathrm{k}} \left(z_{\mathrm{k}} - C\hat{x}_{\mathrm{k}|\mathrm{k}-1}\right) \tag{42}$$

and updating the error covariance as follows:

$$P_{\mathrm{k}|\mathrm{k}} = (I - K_{\mathrm{k}}C) P_{\mathrm{k}|\mathrm{k}-1} \tag{43}$$

3 Solenoid test and simulation model

3.1 Electromagnet Test Bench

Solenoid test calibration experiments use a self-made electromagnet test bench, mainly composed of the electric servo cylinder, servo control system, solenoid fixing block, solenoid controller, DC power supply, data acquisition device, and other components, shown in fig. 4. The solenoid fixed block can maintain the overall position of the solenoid unchanged. The servo control system controls the expansion and contraction of the electric servo cylinder, which in turn can control the position of the solenoid core. The DC power supply powers the proportional solenoid controller, which injects voltage signals into the solenoid, while a current sensor is integrated to obtain the current. The data is uniformly collected and saved by the data acquisition device. In this paper, after the calibration test of the proportional solenoid on the electrohydraulic proportional valve, the simulation model of the solenoid is established. Then, the effect of the dual-solenoid position soft measurement method is verified in the Simulink simulation of MATLAB software.

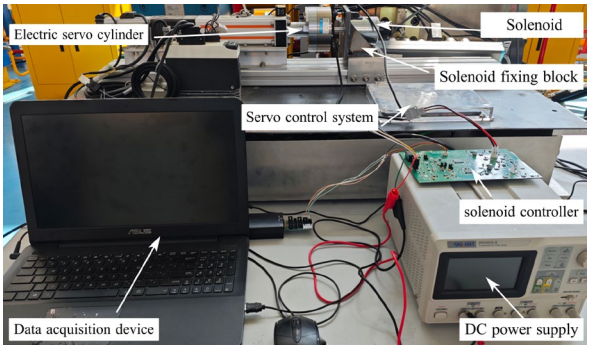

Figure 4: Electromagnet Test Bench

3.2 Solenoid characterization data acquisition and processing

3.2.1 Solenoid simulation model

In this paper, a solenoid simulation model is established, as shown in fig. 5, and the specific establishment method is described in detail in the previous research results [16-17]. The test temperature of the solenoid is room temperature. For the solenoid to apply voltage excitation to obtain data, it is quickly completed, so do not consider the solenoid operation process temperature changes on the resistance.

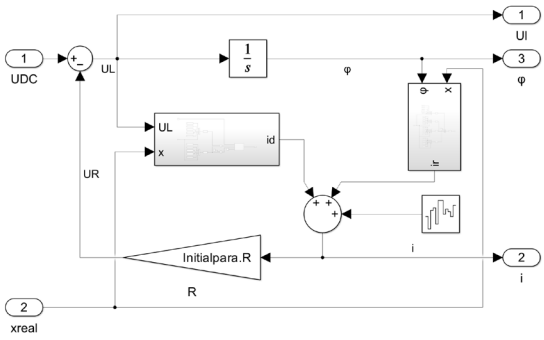

Figure 5: Solenoid simulation model

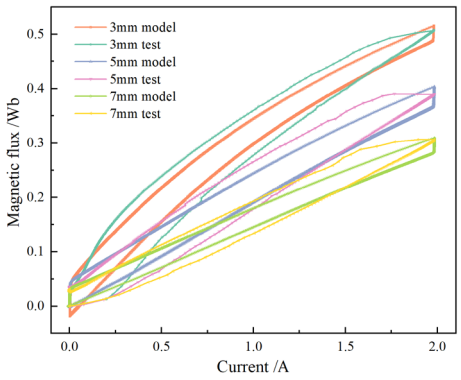

Figure 6: Comparison of solenoid test and simulation

Fig. 6 shows that when the 0-9 V step voltage command is applied to the solenoid model, the response current and magnetic flux change the relationship. Compared with the test data, the fitted solenoid simulation model can represent the performance of the actual solenoid and reflect the change rule of the current and magnetic flux. Therefore, the follow-up will be based on this solenoid model to carry out the dual-solenoid position soft measurement method effect verification.

3.2.2 Structure parameters of solenoid

In the self-sensing model of the working solenoid, the necessary parameters can be obtained from the valve manufacturer or by disassembling the solenoid for measurement. In a more general implementation, the solenoid parameters should be provided by the valve manufacturer during production. This integration eliminates the need for additional measurements of the solenoid's structural characteristics, thereby streamlining the design and manufacturing process. However, in this paper, the size parameters of the solenoid are obtained by disassembling it and are listed in tab. 1. After checking the samples, the rated stroke of the solenoid is 4 mm. The core is compressed inward by 3 mm from the outermost end to the compression of 7 mm, which is the working interval. Therefore, the subsequent position soft measurement simulation is also carried out in this interval.

Table 1: Structure parameters of solenoid

Parameters	Value	Parameters	Value
r_{21}, r_{41}	15.80	l_3	0.0285
r_{22}, r_{42}	15.70	N	780
l_2, l_4	0.006	A_s	443.35e-06
r_{31}	12.65	R	5.07
r_{32}	12.50		

3.2.3 Calibrating idle solenoid inductance and position

The calibration of the inductance and position relationship of the idle solenoid is carried out using the electromagnet test bench, which is necessary for the idle solenoid to measure the position. According to the test, under the existing control board hardware facilities, the solenoid response to excitation is best

when the input excitation voltage amplitude is 0.5 V, the bias is 0.5 V (i.e., the voltage fluctuates between 0 and 1 V), and the frequency is 100 Hz. The current amplitude shows the most pronounced monotonic change with increasing air gap length. As shown in fig. 7, a quartic curve was selected to fit the inductance and position relationship after comparing the effects of the quadratic, cubic, and quartic curve fits. The final fitting parameters are shown in tab. 2.

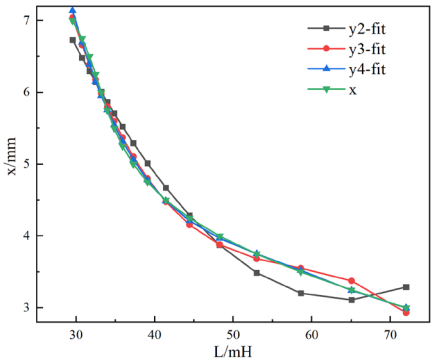

Figure 7: Inductance-position fitting

3.3 Dual-solenoid position soft measurement simulation model

According to the dual-solenoid position soft measurement method derived in Section 2, combined with the solenoid model already established in Section 3.2, the Simulink model of the dual-solenoid position soft measurement method simulation is built, as shown in fig. 8.

Fig. 8 shows the dual-solenoid position soft measurement method model. The purple part in the figure is the input signal module, which will generate sine and step position signal commands in the next section of the simulation. The green part in the figure is the working solenoid position self-sensing module, which inputs a 9 V voltage step signal at the beginning of position sensing (at 0.5 s) to generate the initial excitation and maintain the solenoid in the energized state. The equivalent inductance voltage, current, and flux signals of the solenoid are input into the position self-sensing model to output the position of the solenoid x_1. The yellow part in the figure is the idle solenoid position sensing module, to which a sinusoidal excitation signal is continuously applied with the voltage selection, as mentioned in Section 3.2.3. The current is acquired as the input to the subsequent idle solenoid position estimation module, and the final output is the position x_2. The

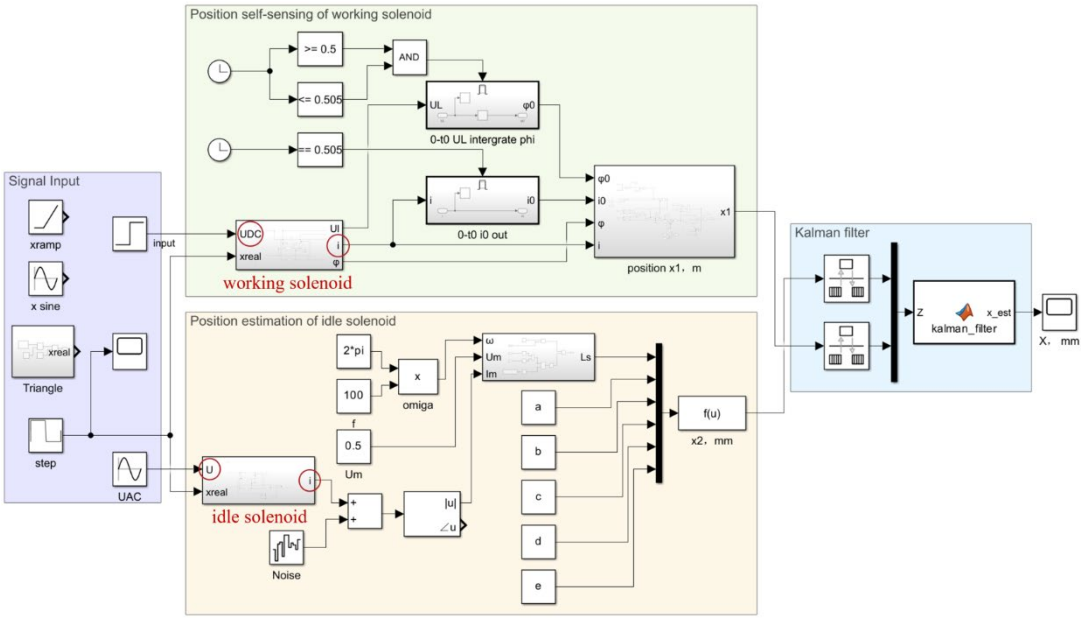

Figure 8: The simulation model of the dual-solenoid position soft measurement method

Table 2: Inductance-position fitting parameters of idle solenoid

Parameters	Value
a	3.4588e-06
b	-8.1919e-04
c	0.0724
d	-2.8758
e	47.3696

necessary parameters required for the dual solenoids soft measurement method are labeled in the figure. The system captures and archives the input voltage (DC for the working solenoid and AC for the idle solenoid) along with the corresponding response current for subsequent processing. Concurrently, other variables, such as magnetic flux and inductance voltage, are computed by integrating these acquired measurements with the solenoid pre-measured parameters, as described in Section 2. The blue part in the figure is the data fusion output module using the adaptive Kalman filtering method, where x_1 is used as the predicted value input and x_2 is used as the observed value input.

4 Simulations

4.1 Sinusoidal signal simulation

In this simulation, the input solenoid position is sinusoidally varied according to the interval of 3 mm - 7 mm with a variation frequency of 0.5 Hz. Fig. 9 shows the effect of position soft measurement when no noise is added. The position estimation results of the working solenoid and the idle solenoid can both accurately obtain the initial value and follow the actual position change. In more detail, the estimation results of the idle solenoid stabilize faster than those of the working solenoid. The fused results are closer to the actual value, and the accuracy is 1.91% after the measurement is stabilized.

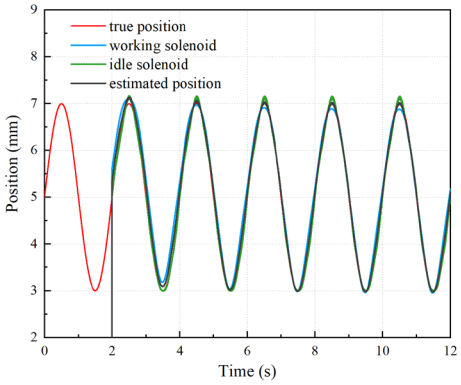

Figure 9: Sinusoidal signal simulation position estimation results (no noise)

Then, Gaussian white noise with a mean of 0 and a standard deviation of 0.005 A is added to the current sample of the solenoid model to simulate the measurement error of the current sensor due to inaccuracy in the actual application process and to verify the anti-interference ability of the model. Fig. 10(a) and 10(b) show that the estimation results of the working solenoid are more noise-resistant than those of the idle solenoid. After adaptive Kalman filter data fusion, the position soft measurements are well denoised and more closely match the actual displacement values than the individual estimates from either solenoid. The average accuracy of the position measurement remains within 6%, and the accuracy is slightly worse when the curve changes direction because the measured value of the working solenoid is somewhat different from the actual value, which affects the final result of the soft measurement to some extent.

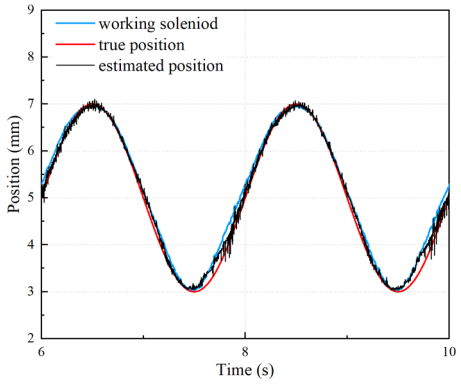

(a)

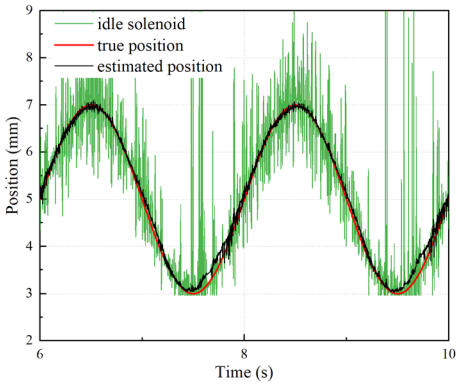

(b)

Figure 10: Sinusoidal signal simulation position estimation results (with noise)

4.2 Step signal simulation

In this simulation, the input solenoid position is made a step change between the position of 4 mm and 6 mm with a period of 2 s. Fig. 11(a) shows the effect of the position soft measurement method. The measured position follows the actual position change better, and the position soft measurement accuracy is within 2.33% of the whole stroke at the smooth time. Due to the inductance of the working solenoid being calculated iteratively, it is susceptible to a large error at the time of position switching. From fig. 11(b), it can be seen that this problem can be effectively mitigated by the dual-solenoid soft measurement method.

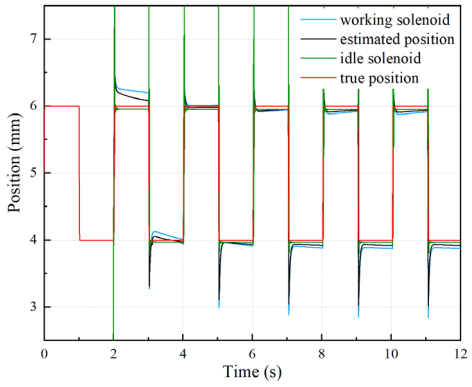

(a)

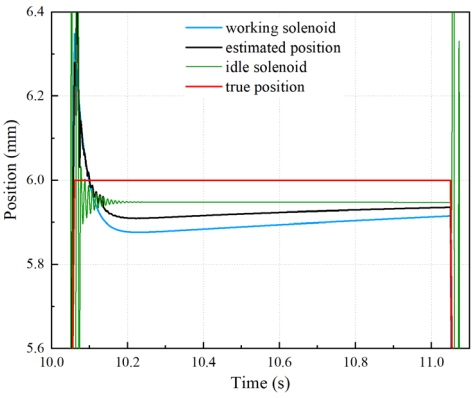

(b)

Figure 11: Step signal simulation position estimation results (no noise)

Similarly, Gaussian white noise with a mean value of 0 and a standard deviation of 0.005 A was later added to the current samples of the solenoid model to verify the noise immunity of the model. A comparison of fig. 12(a) and 12(b) show that the position soft measurements after data fusion by adaptive Kalman filtering have a good denoising effect. The accuracy is 2.06% after the measurement is stabilized. Similarly, the impact on the working solenoid due to the sudden change in position generation during the step is mitigated, as can be clearly seen in fig. 12(b).

In the step signal simulation, the results also indicate that the position estimation method based on the idle solenoid exhibits a faster dynamic response, whereas the method based on the working solenoid demonstrates superior robustness against noise. The dual-solenoid position soft measurement method proposed in this study effectively integrates the strengths of both methods, leading to improved estimation accuracy.

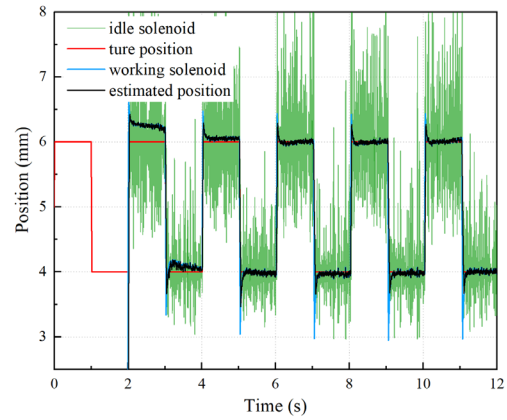

(a)

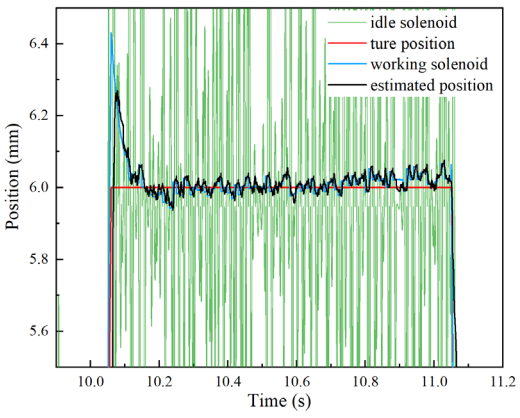

(b)

Figure 12: Step signal simulation position estimation results (with noise)

5 Conclusion

This paper proposes a position soft measurement method based on dual solenoid data fusion to realize an accurate estimation of spool position. The method solves the problems of inaccuracy, low adaptability, and susceptibility to noise interference brought by a single solenoid. Besides, the method utilizes only the original parts of the solenoid valve without adding additional auxiliary components. After prior calibration, it can realize the effect of accurately detecting the initial position and precisely following the position change. Simulation results demonstrate that the soft measurement method based on dual-solenoid position data fusion yields promising outcomes under various operating conditions. In noise-free scenarios, the measurement accuracy after stabilization remains within 2.5% of the full stroke. When subjected to Gaussian noise interference with a standard deviation of 5 mA, the method demonstrates strong noise immunity, ensuring accurate position identification across most of the stroke. Although a transient degradation in precision (exceeding 5%) is observed during spool directional reversals, the system rapidly recovers to yield correct measurements. Currently, proportional valves without displacement sensors but with mechanical hydraulic feedback achieve ±1% accuracy and under 3% hysteresis. The performance achieved by the method proposed in this paper nearly meets this criterion, indicating its potential to replace conventional valves for improved automation in production processes. Moreover, this advancement can facilitate condition monitoring and support fault diagnosis applications, such as detecting spool sticking.

The method proposed in this paper is specifically for dual-solenoid proportional valves, where the coordinated operation of two solenoids enables the final position estimation. This dual-solenoid configuration effectively compensates for the shortcomings inherent in single-solenoid systems. In the industrial applications where valves are equipped with a single solenoid, the working solenoid position estimation method may be more suitable for simultaneously achieving both force generation and position sensing. It is critical to ensure the accuracy of the solenoid's structural parameters, as the position calculation relies on data from the solenoid. Simulation results show that the working solenoid method exhibits greater resilience to noise. Conversely, although the idle solenoid method operates independently of the structural parameters, it is more sensitive to the noise and requires additional filtering to mitigate noise interference. Besides, if this approach were to be applied to a single-solenoid valve, it would necessitate a redesign of the valve structure to incorporate an auxiliary coil for sensing the changes in inductance.

As the use effect of this study has mainly been conducted using an established solenoid model, future experiments will be carried out on a valve equipped with a displacement sensor. The sensor data will be compared to validate the efficacy of the dual-solenoid position soft measurement method. Additionally, the prolonged operation of the solenoid may lead to an increase in temperature, which could theoretically affect both the resistance and the accuracy of the position estimation. Therefore, future work will need to address the impact of temperature variations on these parameters.

Nomenclature

Designation	Denotation	Unit
R_1, R_2, R_3, R_4	Magnetic reluctance of air gaps 1, 2, 3, and 4	1/H

x_1	Position of the iron core /Length of air gap 1	m
μ_0	Hydraulic oil magnetic permeability	H/m
A_s	Cross-sectional area of air gap 1	m^2
r_{21}, r_{31}, r_{41}	Outer radius of air gaps 2, 3, and 4	mm
r_{22}, r_{32}, r_{42}	Inner radius of air gaps 2, 3, and 4	mm
l_2, l_3, l_4	Length of air gaps 2, 3, and 4	m
R_5	Armature magnetic reluctance	1/H
R_6	Yoke magnetic reluctance	1/H
ψ	Working solenoid magnetic flux linkage	Wb
N	Coil turns	/
ϕ_1	Average magnetic flux	Wb
L_w	Working solenoid inductance	H
I_w	Working solenoid current	A
U_{DC}	DC supply voltage	V
U_L	Working solenoid inductive voltage	V
U_R	Working solenoid resistive voltage	V
R	Coil resistance	Ω
ψ_0	Working solenoid initial magnetic flux linkage	Wb
L_0	Working solenoid initial inductance	H
i_0	Working solenoid initial current	A
t_0	Initial voltage generation time	s
Δt	Time increment	s
δ_0	Initial armature position	m
$\Delta\psi$	Magnetic flux linkage variation	Wb
L_1	Inductance after the L_0	H
Δi	Current variation	A
i_{k-1}	Current at the previous time step	A
L_{k-1}	Inductance at the previous time step	H
L_k	Present inductance	H
Δx	Position variation	m
U_{AC}	AC supply voltage	V
$\bar{U}_m$	AC voltage amplitude	V
ω	Angular frequency	rad/s
U_k	DC offset of the AC voltage	V
I_{AC}	Response current	A
$\bar{I}_m$	Response current amplitude	A
θ	Phase lag between the current and voltage	degree
I_k	DC offset of the response current	A
ϕ_2	Idle solenoid magnetic flux	Wb
L_s	Idle solenoid inductance	H
x_2	Estimated position of the idle solenoid	m
a, b, c, d, e	Coefficients of the quartic fitting polynomial	/
X_k	State vector	/
x_k	Solenoid core displacement	m
v_k	Solenoid core velocity	m/s
T	Sampling period	s
A	State transition matrix	/
Q_k	Process noise covariance	/
w_{k-1}	Process noise vector	/
$z_{1,k}$	Working solenoid position x_1	m
$z_{2,k}$	Idle solenoid position x_2	m
C	Observation matrix	/
z_k	Observation equation	/
R_k	Observation noise covariance	/
R_{base}	Initial observation noise covariance	/
r_{base1}, r_{base2}	Initial observation noise covariance parameters	/
x_{Ru}, x_{Rl}	Upper and lower segmentation points of the difference between $z_{2,k}$ and $z_{1,k}$	m
q_{k1}, q_{k2}, … q_{k6}	Process noise covariance parameters	/
x_{Qu}, x_{Ql}	Upper and lower segmentation points of the difference between x_2 and current estimation	m
α	Fusion factor	/
s_{err}	Step error	m
n_L	Noise level	m
ε	Small constant to prevent the denominator from being zero	/
P_x	Error covariance	/
$\hat{x}_k$	Final estimated position	m

Acknowledge

This work was supported by the State Key Program of National Natural Science of China (509116-N12501ZJ).

References

[1] M Yang, K Lian, S Luo and et al. Simulation analysis and optimization of pilot type electro-hydraulic proportional directional valve based on multi field coupling. Flow Measurement and Instrumentation, 100:102726, 2024.

[2] J Ren, B Zhao, L Quan, et al. Research on proportional valve spool wear diagnostic method hybrid-driven by the valve port energy loss mechanism model and data. Mechanical Systems and Signal Processing, 219:111606, 2024.

[3] J Shen, H Zong, M Cheng and et al. Force soft measurement based on cylinder decoupling model and stepwise parameter identification for hydraulic manipulators. IEEE Transactions on Instrumentation and Measurement, 73:7504912, 2024.

[4] W Ma, L Tan, H Feng, et al. A data-driven LSTM soft sensor model based on Bayesian optimization for hydraulic pressure measurement of excavator. IEEE Sensors Journal, 23(21):25749-25759, 2023.

[5] D Xie, Y Yang, Y Zhang and et al. Precision positioning based on temperature dependence self-sensing magnetostrictive actuation mechanism. International Journal of Mechanical Sciences, 272:109174, 2024.

[6] H C Pedersen, T Bak-Jensen, R H Jessen, et al. Temperature-independent fault detection of solenoid-actuated proportional valve. IEEE/ASME Transactions on Mechatronics, 27(6):4497-4506, 2022.

[7] B A Reinholz and R J Seethaler. Sensor fusion of self-sensed measurements for position control of a constant air-gap solenoid. IEEE Sensors Journal, 22(24):23997-24005, 2022.

[8] S Nagai, T Nozaki and A Kawamura. Environmental robust position control for compact solenoid actuators by sensorless simultaneous estimation of position and force. IEEE Transactions on Industrial Electronics, 63(8):5078-5086, 2016.

[9] S Nagai and A Kawamura. Position sensorless position control for dual solenoid actuator. Proc. of 2018 International Power Electronics Conference (IPEC-Niigata 2018 -ECCE Asia), 1687-1691, 2018.

[10] T Kramer and J Weber. Self-sensing design of proportional solenoids. Proc. of Proceedings of the BATH/ASME 2020 Symposium on Fluid Power and Motion Control, 2811, 2020.

[11] T Braun, J Reuter and J Rudolph. Observer design for self-sensing of solenoid actuators with application to soft landing. IEEE Transactions on Control Systems Technology, 27(4):1720-1727, 2019.

[12] X Zhao, L Li, J Song, et al. Linear control of switching valve in vehicle hydraulic control unit based on sensorless solenoid position estimation. IEEE Transactions on Industrial Electronics, 63(7):4073-4085, 2016.

[13] G Cao， H Hu, S Huang et al. An assistant-mover-based position estimation method for planar switched reluctance motors. IEEE Transactions on Industrial Electronics, 67(7):6066-6077, 2020.

[14] Y Jing, S Wang, Q Liu et al. Gap self-sensing method for maglev system using partial electromagnet coil. IEEE Transactions on Industrial Electronics, 71(4):4273-4282, 2024.

[15] M Verma, V Lafarga, and C Collette. Perfect collocation using self-sensing electromagnetic actuator: Application to vibration control of flexible structures. Sensors and Actuators A: Physical, 313: 112210, 2020.

[16] J Fang, X Kong, X Zhu, et al. The modeling and experimental verification of a servo-proportional valve. Applied Mechanics and Materials, 220-223:1018-1022, 2012.

[17] B Xu, Z Lu, J Zhang, et al. Dynamic experiment and modeling of a proportional solenoid electromagnet. Chinese Hydraulics & Pneumatics. 9:1-5, 2015.